7. OSS IV: NOISE LEVELS, SIGNAL-TO-NOISE RATIOS, AND NOISE SOURCES[1]

Fred K. Duennebier, Charles S. McCreery, David Harris, Robert K. Cessaro, Craig Fisher, and Paul Anderson,
Hawaii Institute of Geophysics[2]

ABSTRACT

The ocean sub-bottom seismometer (OSS IV) is one of the quietest seismic stations in the world at frequencies between 4 and 15 Hz. Noise levels of 10^{-12} m^2/Hz are observed above 4 Hz. Noise at frequencies above 5 Hz appears to be caused by system noise during quiet periods, but is dominated by storms at other times. Ships, whales, and earthquakes also add to the noise. The equivalent acoustic noise level varies between 60 and 70 dB re 1 μPa, about 10 to 20 dB quieter than the ocean. Signals generated in the ocean can be observed out to long distances, with propagation loss on the order of 120 dB (referenced to a source level at 1 m) at 100 km. Signals generated from earthquakes are observed about once per hour with signal-to-noise ratios and fidelity considerably improved over those obtained from ocean bottom seismometers. Bottom loss measurements indicate that acoustic signal amplitudes decrease by slightly less than a factor of two with every reflection from the ocean bottom at pre-critical angles.

INTRODUCTION

Noise levels, signal-to-noise ratios (S/N), noise sources, and signal propagation have been quantized for the ocean sub-bottom seismometer (OSS IV). The OSS IV was emplaced in Hole 581C in September 1982, and noise levels were recorded continuously for 64 days. The question, "Do increases in signal fidelity and S/N down the hole—versus sensors in the ocean or on the ocean floor—justify the cost of emplacing seismic sensors in ocean drill holes?," must be answered before more experiments are seriously considered. In this chapter, we present preliminary results from OSS IV noise and signal-propagation studies that document the increase in fidelity and S/N obtained at this site. We believe that the results justify further experiments.

Other experiments have obtained ocean acoustic and seismic noise levels (Urick, 1983; Nichols, 1981, Carter et al., 1984; Adair et at., 1984) with acoustic levels at 10 Hz commonly between 80 and 90 dB re 1μPa/Hz, and seismic levels on the ocean floor as low as 20 pm/Hz, but normally above 100 pm/Hz (rms). Note that 1 pm = 1 picometer = 10^{-12} m. Carter et al. (1984) found that equivalent noise levels near 100 pm/Hz were found on an ocean bottom seismometer (OBS) and another ocean sub-bottom seismometer (OSS II) when an impedance correction was applied to the OSS data. The OSS II was emplaced in soft sediment 194 m below the OBS. The marine seismic system (MSS) experiment in 1981 achieved noise levels of about 500 pm/Hz at 2 Hz but did not obtain data above 2 Hz (Adair et al., 1984). Data from the MSS experiment on DSDP Leg 91 are reported in this volume (Orcutt et al.).

When comparing noise levels, it is important to take into account the elastic properties of the material in which the noise is measured. Since energy is proportional to the density and wave velocity of the material (ρc, the acoustic impedance), particle motion amplitudes will vary as the square root of the impedance (Carter et al., 1984). Thus noise levels in dense, high velocity material will be deceptively lower that those in low density, low velocity material. When comparing different systems in different media, a correction should be applied.

INSTRUMENT DESCRIPTIONS

A detailed instrument description of the OSS borehole seismic system is found in Byrne et al. (this volume). The instrument at Site 581 was emplaced on 11 September 1982, in 5467 m of water at the bottom of Hole 581C. The hole drilled through 356 m of sediment and about 22 m of basalt. The instrument rests in the bottom of the hole and is strongly clamped by a spring in a near-vertical ($<4°$) position. The instrument contains orthogonal 4.5 Hz geophone stacks wired in series, nine in the vertical stack and two in each horizontal stack.

The data are digitized in the borehole tool. Each digital word contains a 9-bit mantissa and a 3-bit (base 4) exponent for a total dynamic range of 138 dB and resolution to greater than 0.8%. Sample rates are either 100 Hz or 50 Hz per channel depending on the power level sent to the tool. When a ship is monitoring the end of the cable connected to the tool in the hole, the data are digitized at 100 samples/s. When the recording package is attached to the cable, data are sampled at 50 samples/s.

In the real-time mode, data are recorded on board ship in digital form and no fidelity is lost. When the recorder package is attached, the data are converted back to analog format for continuous recording. The conversion to analog involves loss of dynamic range (about 40 dB) extended to 120 dB by automatic gain control allowed to change once per minute. The analog recorded signal suffers from clipping when transient signals exceed the dynamic range, but suffers only minor loss of fidelity when signal (and noise) levels are relatively small.

---

[1] Duennebier, F. K., Stephen, R., Gettrust, J. F., et al., *Init. Repts. DSDP*, 88: Washington (U.S. Govt. Printing Office).

[2] Address: Hawaii Institute of Geophysics, University of Hawaii, 2525 Correa Rd., Honolulu, HI 96822.

The OSS IV horizontal sensors have been oriented by shot azimuth studies. One geophone (Ch. 1) is oriented with its positive axis at 89° east of north ± 1.5° (Anderson et al., in press), and the other is orthogonal (positive south). This analysis also requires that Hole 581C be about 500 m west of the drillship location during drilling. The corrected hole location is 43.9240°N, 159.7909°E.

Ten ocean bottom seismometers (OBS) were emplaced at and near the drill site. Five were HIG Isolated Sensor Ocean Bottom Seismometers (ISOBS), and five were Oregon State University OBSs. All HIG OBSs recorded data in analog format with transfer functions similar to the OSS geophones (Fig. 1). Data from hydrophones, vertical geophones, and an unoriented horizontal geophone are recorded by each OBS. The OSU instruments have the seismic sensors contained in the same package as the tape recorders and flotation, whereas the HIG OBS's deploy the geophones in a small package about 1 m from the flotation and recorders. This isolation of the sensors improves fidelity of ground-motion detection and decreases noise (Byrne et al., 1983).

Two of the HIG OBSs were within 500 m of Hole 581C, the others were approximately 40 km to the south, east, and west. The OSU OBSs were about 5 km from the borehole, also to the south, east, and west.

RESULTS

This report is divided into several sections dealing with the noise and propagation effects observed at the OSS IV site. First, absolute noise levels obtained from the OSS early in the experiment are compared with those from an OBS for the same time period, and the temporal variation of noise over the 64-day analog-recording period is discussed. The origin and characteristics of the noise and the known sources of noise are also discussed in this section. In the next section, the signal-to-noise ratio (S/N) is evaluated for both earthquakes and acoustic sources in the ocean, and propagation loss for acoustic sources is evaluated. Lastly, preliminary conclusions are drawn concerning the value of ocean borehole seismic/acoustic sensors.

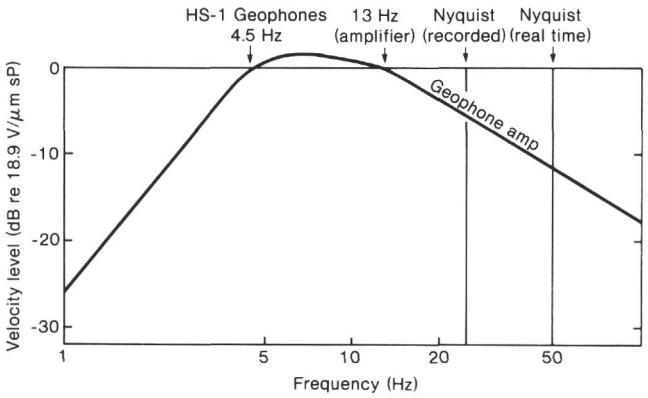

Figure 1. System response curve for the Ocean Sub-bottom Seismometer geophones. The ocean bottom seismometer geophones have similar response curves.

Absolute Noise Levels, Temporal Variation of Noise, and Noise Sources

Absolute noise level measurements were obtained from two OBSs and the OSS shortly after the emplacement of OSS IV when data were being recorded in the digital format. Sample noise spectra are shown in Figure 2. The OSS vertical component noise level is more that 20 dB quieter that the OBS levels over most of the frequency band. Note the similarity between the HIG ISOBS spectrum and the OSS spectrum. Both show similar spectral peaks and shapes, although the OSS spectrum has a better S/N for the peak at 20 Hz (generated by the nearby *Glomar Challenger*) than the ISOBS. The Oregon State University OBS spectrum was taken a few hours later and does not show the same structure. This large difference between the spectral properties of the OSU OBS and the other two instruments is not known. To correct for the difference in impedance between the basalt in the borehole (ρ = 2.3 g/cm^3, c = 3.0 km/s) and the sediment under the OBS (ρ = 1.3 g/cm^3, c = 1.6 km/s) the OSS curve should be raised by 5.2 dB.

A more striking difference in noise levels is seen between the OSS and ISOBS horizontal components (Fig. 3). In this case, the difference in noise levels is nearly 30 dB across the spectrum. The OSS IV horizontal noise levels are about the same as the vertical levels shown in Figure 2, but the ISOBS horizontal is about 10 dB noisier than the vertical levels. This extra noise is probably

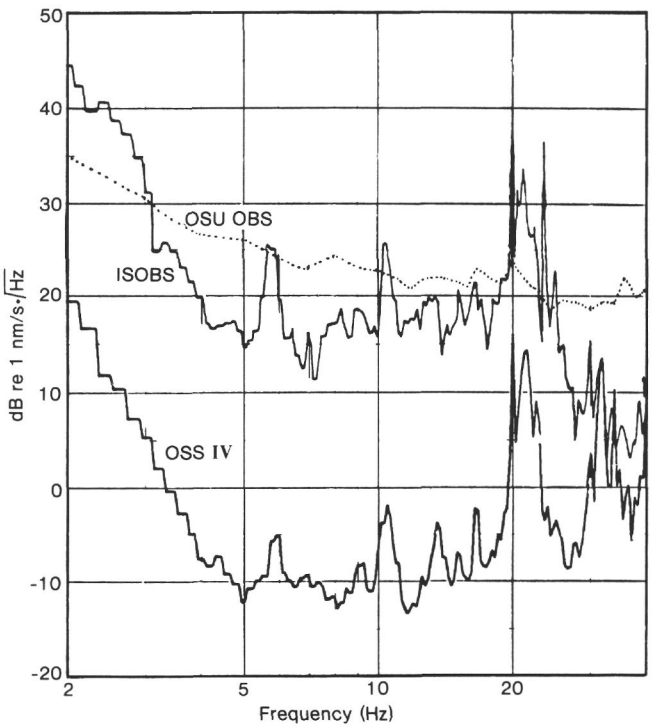

Figure 2. A comparison of noise levels recorded by the vertical-component geophones of the OSS, and noise levels recorded by two OBSs during the emplacement phase of OSS IV. Spectra were taken on Day 254, 1982 at 0185Z for a 30-s period.

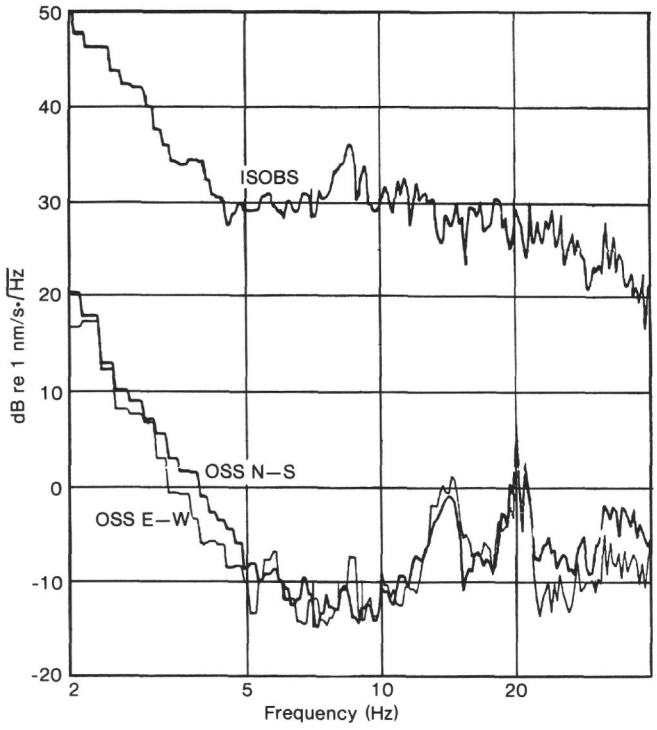

Figure 3. A comparison of noise levels recorded by the horizontal component geophones of the OSS IV and ISOBS. Spectra were taken by Julian Day 254, 1982 at 0815Z for a 30-s period.

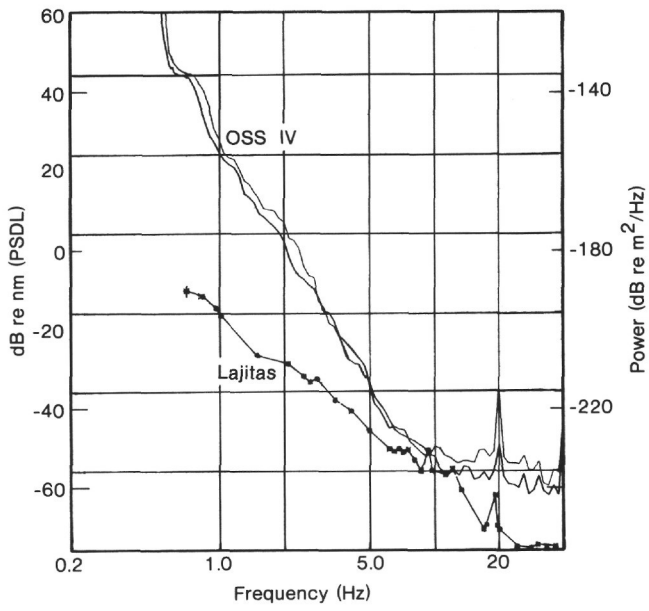

Figure 4. A comparison of OSS noise levels measured 9 months after emplacement with those from a quiet continental seismic borehole station (Lajitas) (Herrin, 1982). The two OSS curves are the vertical and one of the horizontal components. The other horizontal component was nearly the same as the other two components. (Bandwidth = 1.0 Hz.)

caused by high-amplitude shear energy in the shear wave guide at the top of the sediments. As shear waves approach the water/sediment boundary from below, their velocity decreases from about 1.6 km/s in the ocean crust to less that 50 m/s at the ocean floor. This decrease reduces the wavelengths by more than a factor of 30 and increases amplitudes (assuming no other losses) by about 17 dB (ρ = 2.3, v_p = 1.6 in the crust, and ρ = 1.3, v_s = 0.05 at the ocean floor). The very low velocity also results in all shear ground motion being nearly horizontally polarized at the ocean floor. The very short wavelengths make the shear waves prone to scattering by relatively short wavelength and low-angle undulations on the ocean floor. Even a slight change in angle will trap energy in the sediments that would otherwise have returned to the ocean crust.

During recovery of the recording package 9 months after emplacement of OSS IV, noise levels were again measured and found to be about 10 dB lower than those measured during emplacement. This quieting probably represents a combination of filling in of the drill hole and better weather. In Figure 4, the OSS noise levels from the analog recorded data (during a relatively quiet period) are compared with the Lajitas continental borehole station in Texas (Herrin, 1982). The OSS IV noise level increases at about 20 dB/octave with decreasing frequency below 6 Hz and levels out above 6 Hz. The continental noise levels increase at about 12 dB/octave below 20 Hz. In both cases, the leveling of the noise at high frequencies may be caused by system noise rather than seismic noise. The difference at the low frequency end of the spectrum is most likely the result of coupling of ocean waves above the OSS into the motion of the ocean floor (Duennebier et al., in press). If this is the case, noise level will change in response to changes in ocean swell and storm waves.

Temporal changes in noise level were measured by OSS IV during a continuous 64-day period from 12 September 1982 to 16 November 1982. These data were recorded on five analog tape cassettes recovered on 26 May 1983 (Byrne et al., this volume). Processing to obtain spectral noise levels was accomplished by passing the analog signals through an H-P 3582-A Spectrum Analyzer and capturing the digital spectral output (2 spectra averaged every 28 min.). See the Appendix for details of data reduction for Figure 5. These spectra were averaged and filtered to obtain signal levels in six frequency bands for the two horizontal axes. Also plotted are the atmospheric pressure and pressure gradient measured by hand from weather (surface pressure) maps every 12 hr. Measurements plotted represent crude averages for a region about 100 km in diameter around Site 581. There is a strong correlation between high atmospheric pressure gradients and high noise levels above 4 Hz. High pressure gradients indicate the passage of storms over the site, and thus indicate that borehole noise levels can be increased by as much as 12 to 18 dB by storm-wave activity at the ocean surface. The sensitivity of the instrument to acoustic "noise" is also demonstrated by the fact that the splash from 6-lb. SUS charge dropped from a P-3 aircraft directly over the hole was well recorded by the vertical geophone.

Also of interest in Figure 5 are the variations in low frequency noise. Near day 280, for instance, a drop of almost 12 dB occurs at frequencies below 6 Hz, lasting

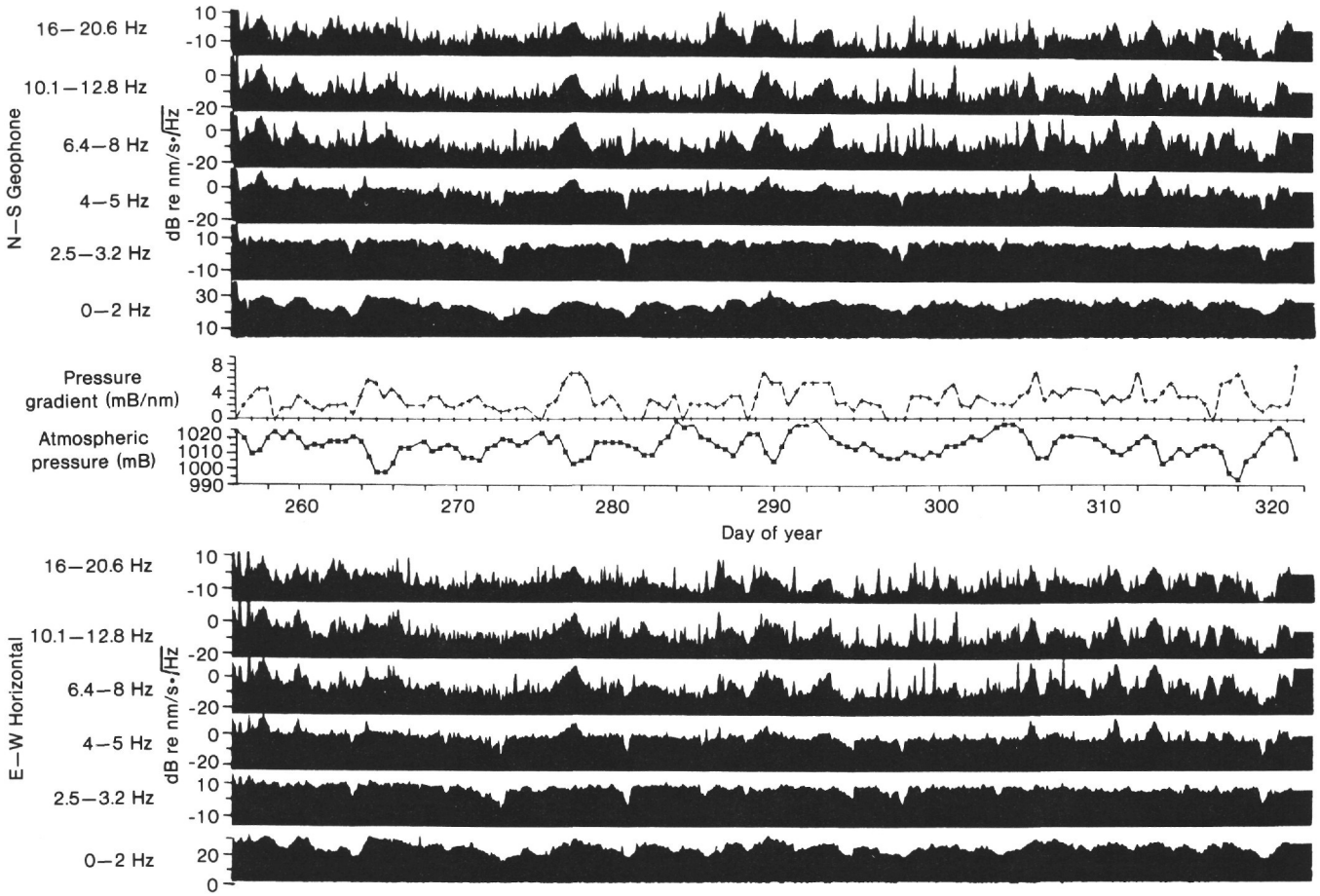

Figure 5. Temporal variation of the seismic background noise at the OSS IV site. The noise levels for the two horizontal geophones are shown in various frequency bands and compared with atmospheric pressure and pressure-gradient fluctuations over the 64-day recording period.

for about 5 hr. at 5 Hz, 8 hr. at 3 Hz, and more than 10 hr. below 2 Hz. Drops in noise level of this type occur several times in the record correlating with atmospheric pressure highs and pressure gradient lows, thus possibly correlating with very quiet sea conditions. A detailed analysis of these variations is given in Duennebier et al., (in press). They demonstrate a strong correlation of noise level spectrum in the borehole with the ocean-wave spectrum deduced from the atmospheric pressure gradient.

The peaks lasting for several hours on the record are noise caused by the passage of ships near the site. More than 120 signatures of ships were recorded during the 64-day period, and signals from at least one ship are nearly always visible in the data. A sample spectrogram of data is shown in Figure 6, with frequency on the vertical axis, time on the horizontal axis, and amplitude levels shown by the darkness. Several ship "lines" are visible, one at about 8.25 Hz with multiples at 12.5 and 16.5 Hz, and a second broader peak between 9 and 9.5 Hz. Several earthquakes are visible as vertical black lines in pairs (P and S).

The ships are of interest in that there is enough information in the signal envelopes to determine the ship course with a four-way ambiguity, and ship speed and range if the source level is known. As shown in Figure 7, the signature of a passing ship is much different on each seismic axis. The signal should reach a maximum on the vertical at closest approach, but the horizontals can have two peaks, and will have an amplitude minimum when the ship is at an azimuth perpendicular to the sensitive axis. The smooth curve shows a theoretical fit to these data using a propagation loss function of

$$A = A_0 r^S$$

where A_0 is the source amplitude, r is range, and S is obtained from propagation loss data discussed later. It is likely that studies of the phase correlation between components could resolve the azimuth ambiguity and provide range information.

Another common type of noise observed in the borehole is seen in Figure 6: the pulses at 18 Hz. These pulses are about 8 s in duration with a higher frequency pulse (near 22 Hz) normally followed directly by the lower frequency pulse. The pulses repeat about once every 65 s for 10 to 13 min. and then skip a pulse before starting again. Rectified traces of this type of noise are shown in Figure 8. Similar signals were recorded by Northrop et al. (1971) on hydrophones near Midway. They speculate that the source is a "large biological source" based on its slow speed and meandering path through the hydrophone array. It is surprising that these sources are seen

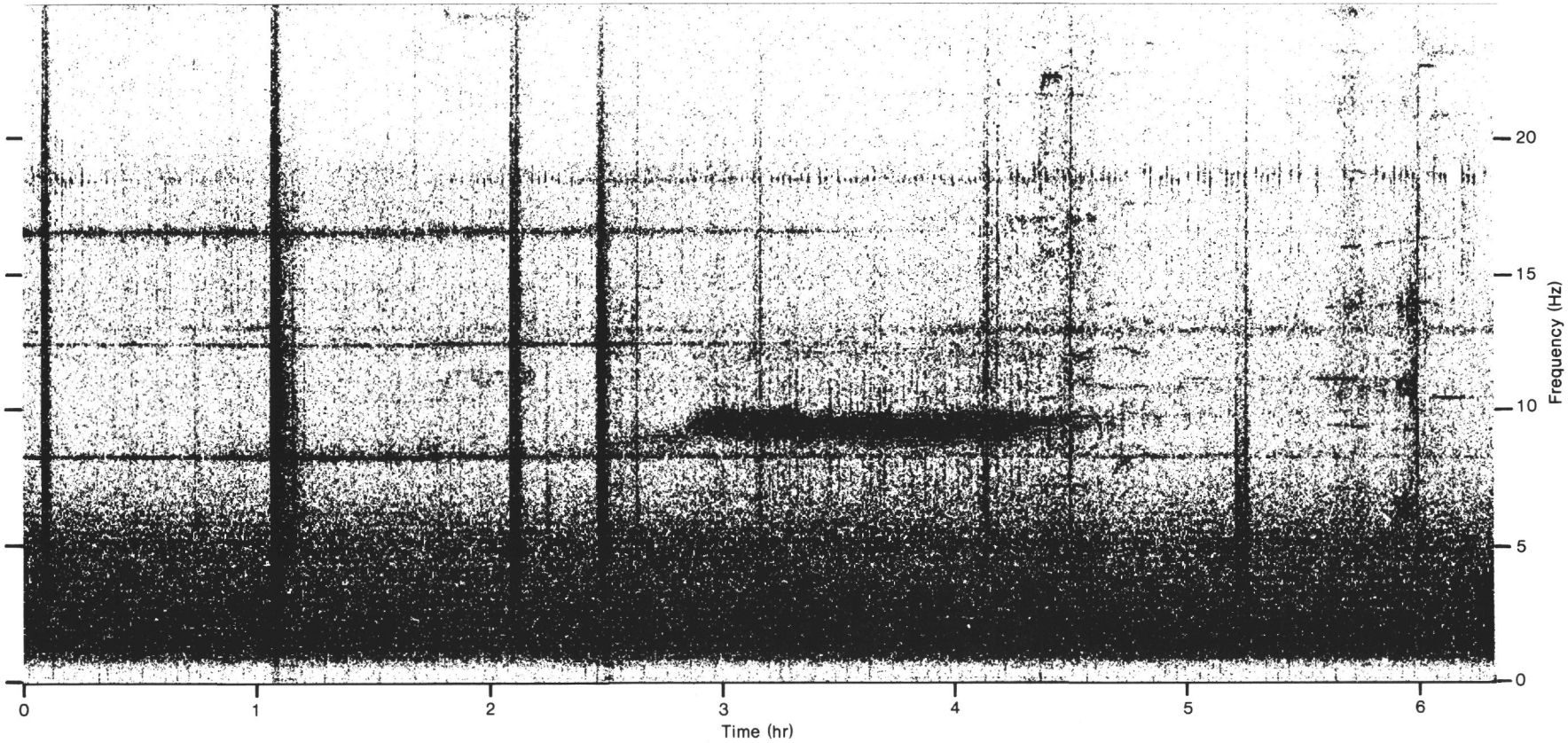

Figure 6. Spectrogram of OSS IV E–W horizontal noise for a 6-hr. period during the 64-day recording period. Dark areas show high signal levels. At least two ships are visible, one with three lines at 8.25, 12.5 and 16.5 Hz, and the other broader band at 9-9.5 Hz. The vertical lines show the arrivals from earthquakes, and the intermittent signals at 18.5 Hz are believed to be from a whale.

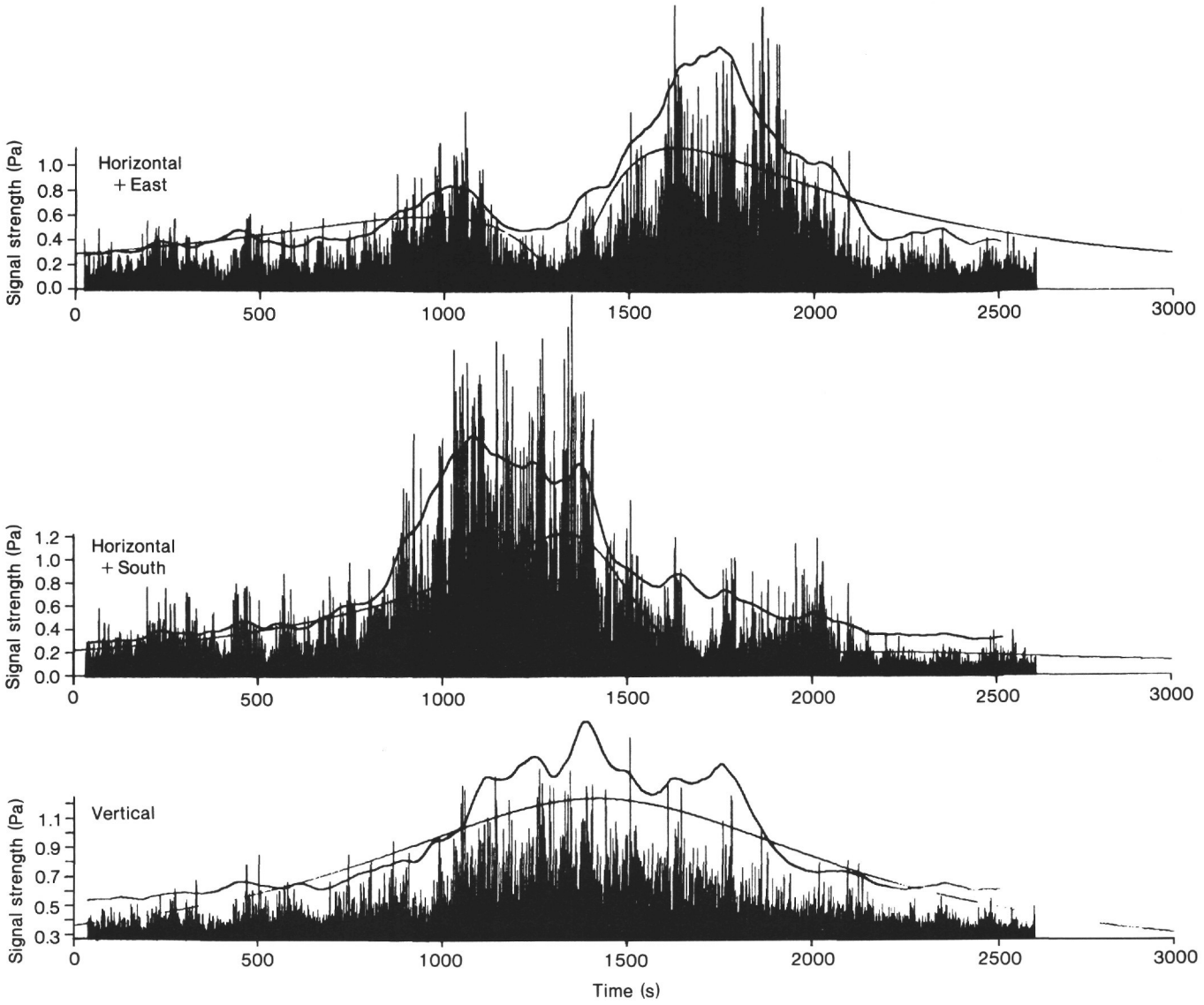

Figure 7. Signal from a ship recorded during the 64-day recording period. Smoothed and unsmoothed rectified traces for the E–W, N–S, and vertical components show the signal at 20 Hz. The smooth curve shows the theoretical amplitude function for a ship on a course of 120° at a speed of 30 km/hr.

with such clarity by sensors 1000 ft. below the ocean floor.

In some studies, earthquakes also become a source of noise. Regional and teleseimic earthquakes with S/N greater that 6 dB were recorded by the OSS IV geophones at a rate of about 1/hr. over the 64-day recording period (Cessaro and Duennebier, this volume). These events span the frequency range from 1 Hz and lower to about 20 Hz and last about 3 min. on average; thus about 5% of the data contain earthquake signals.

When background noise caused by ships, storms, and earthquakes is low, the noise is dominated by instrument-generated noise caused by low-level aliasing of the digital transmission signal. This noise is present when voltages are about 5 μV and below at the input to the analog/digital converter (Byrne et al., this volume). Testing of the system at these levels was not possible because of noise from other sources. It is important to note, however, that true seismic noise is lower than shown by the data at frequencies higher than 5 Hz.

Signal-to-Noise Comparisons and Propagation Loss Analysis

Unfortunately, very little data were collected on ocean bottom seismometers at the same time as OSS IV because the OSS IV emplacement was delayed until the last few days of Leg 88 by the aborted attempt to emplace the Marine Seismic System. One short line of shots was recorded simultaneously on Oregon State University (OSU) OBS(#3) and on OSS IV. The time domain recordings of Shot #503 (35 kg), about 7 km from OBS (#3) and 10 km from OSS IV are shown in Figure 9. First arrivals are well recorded at both stations, but the signals on OSU OBS (#3) are clipped early in the record (starting with the onset of the water wave arrival). Note that both the background and the signal on the OSU

Figure 8. Rectified unfiltered signals believed to be from a "large biological source," recorded on a horizontal OSS IV geophone. The vertical scale is 5 dB per large division. Each trace follows the one above in time. The first peak in each pair has a frequency of about 22 Hz and the second about 19 Hz.

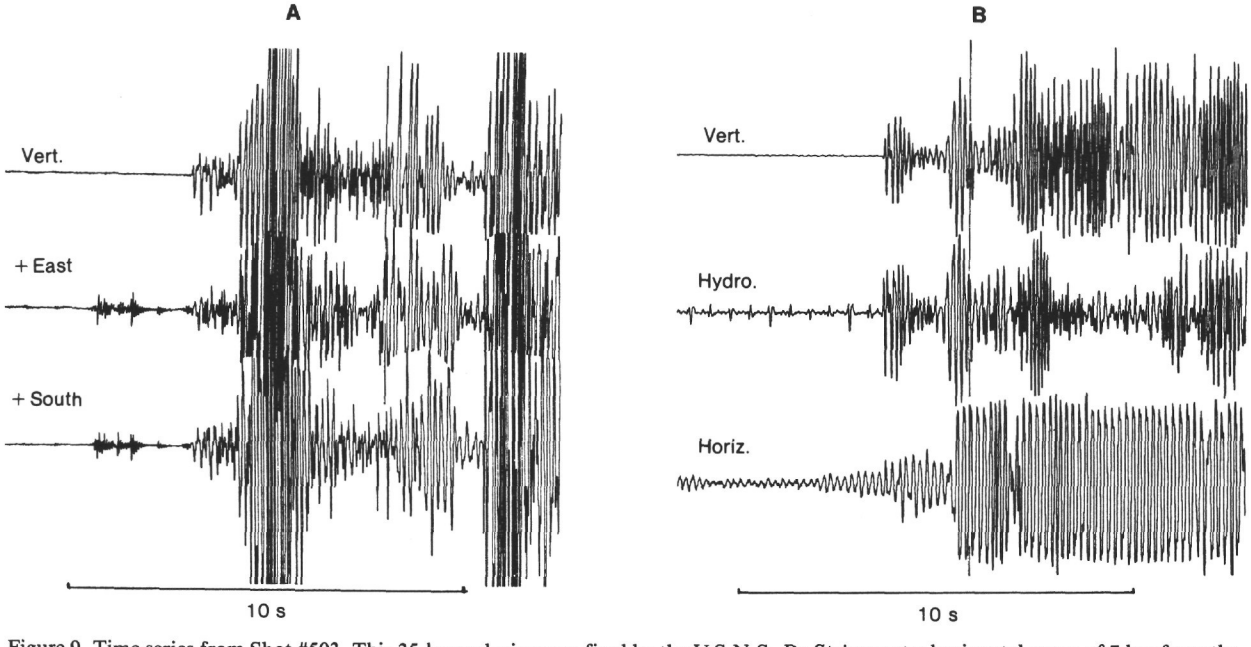

Figure 9. Time series from Shot #503. This 35-kg explosion was fired by the U.S.N.S. *De Steiguer* at a horizontal range of 7 km from the OSU OBS and 11 km from OSS IV. Absolute amplitudes have not been calculated for these traces. They are shown to demonstrate signal quality. A. Signals from OSS IV geophones. The noise in front of the horizontals is caused by material falling down the drill hole. B. OSU OBS signals.

OBS (#3) horizontal components are resonant, with one dominant frequency. Spectra for these recordings are shown in Figure 10 for the first 2 s of signal before the water wave arrival. Note that the OSS IV signals have a broader band signal than the OSU OBS. Signal-to-noise ratios are shown in Figure 11. The OSU OBS vertical S/N is only slightly lower than the OSS between 7 and 15 Hz, but the OSS is far superior at lower and higher frequencies. The dip in S/N on the OSS near 20 Hz is caused by the large 20 Hz noise energy produced by the *Glomar Challenger*. Note also that the S/N on the OBS vertical component is about 18 dB better than on the hydrophone. This difference may be caused by system problems in the OSU OBS. The resonance in the OBS horizontal component is most likely caused by poor coupling with the ocean floor; this is a common problem with ocean bottom seismometers, but one that can be fixed by proper design.

A second example of signals recorded on an ocean bottom seismometer and the ocean sub-bottom seismometer is shown in Figure 12. These are recording of two earthquakes, one made on an ISOBS (Byrne et at., 1983) and one on the OSS recorded in analog format. The one recorded on the ISOBS had a magnitude of 5.0 and a range of 8.1° from the Kuriles, and the one recorded on the OSS had a magnitude of 4.9 and a range of 7.8° from the same region. Comparing the early arrivals (before the signals clip on the analog tapes), the S/N on the vertical components is similar between 4 and 10 Hz, but the OSS seems more sensitive at higher frequencies (Fig. 13).

Unfortunately, there is no direct comparison of arrivals from acoustic signals with all or most of their travel path in the ocean. The ocean bottom seismometers that obtained successful recordings were all analog recordings, and the water wave signals are clipped. An instrument with the ability to digitally record higher dynamic range (OSU OBS) did not operate long enough to make the necessary recording.

An excellent data set was obtained to estimate propagation parameters of acoustic signals to the OSS during the reload of the instrument on 26 May 1984. A circle and two lines of explosives (practice depth charges, PDC Mark 64) were dropped by a Navy P-3 aircraft while the *Kana Keoki* was monitoring the OSS IV borehole package in the digital recording mode. Unfortunately, the circle was not recorded, but excellent data were obtained on a line from 0 to 90 km from the instrument. Each of the 29 (2-ounce) shots fired yields visible signals on the OSS, and the splash of the shot at zero range when the charge hit the water is also visible.

Analysis of these data is important to quantify the detectability of acoustic signals with sources in the ocean. The method used to obtain propagation loss (Fig. 14) is explained in the Appendix. Also given in the Appendix are the transfer functions to change the output of the OSS IV geophones in microvolts to various units of ground motion, pressure, and propagation loss.

The propagation loss curves in Figure 14 show that loss at OSS IV is more than expected from spherical spreading, but the low noise level of the instrument makes it sensitive to sources in the ocean to long ranges. The shot line was from the east, thus less energy is expected on the N-S horizontal component than on the E-W. This is the case over most of the line with the E-W component stronger by about 6 dB. Note that the zero-range shot is about 12 dB stronger on the vertical component than the horizontals. The propagation loss does not seem to vary with frequency in this band, but little change is expected unless attenuation is very high (about 10 dB between 10 and 30 Hz if $Q = 1000$).

It is of interest to determine where the energy is lost, since spreading alone does not account for the loss of signal. In an attempt to determine the mechanism of energy loss we use the intensity of individual acoustic water wave arrivals. In a one-dimensional model we assume that a fraction of the energy is lost from the specular water wave with each ocean bottom reflection, and that another fraction of the energy is lost during transmission through the overlying sediments and basalt before reaching the borehole receiver. The former quantity is known as bottom reflection loss, while the latter quantity is analogously called bottom transmission loss (Fisher, 1986). The amount of energy lost is a function of the reflection (or grazing) angle and frequency.

The analysis was carried out for motion in the radial/vertical plane (for a compressional source in a one-dimensional model, all the energy is contained in compressional and vertically polarized converted shear-wave motions). The data analysis proceeded as follows:

1. Identification of individual water wave arrivals by traveltimes.

2. Calculation of water-wave signal intensity for several frequency bands. At each discrete frequency, the intensity of the water arrival in a 2.56 s time interval was computed. From this arrival intensity the intensity of a noise estimate (recorded a few seconds before) over the same time interval and at the same frequency was subtracted, yielding the signal intensity. The average signal intensity was then computed for the desired frequencies bands.

3. Calculation of the grazing angles (at the water/sediment interface) of the water-wave signals by tracing rays. A water column sound-velocity profile representative of this part of the Pacific Ocean was used (Urick, 1983, Figure 5.16, curve 4). We assume that the bottom-water sound velocity (5.5 km deep) is 1.57 km/s, that the sea bottom and surface are horizontal, and that the dominant reflector for the water waves recorded in the borehole is the sediment/basalt interface (rather than the ocean floor).

4. Computation of average grazing angles for the water wave arrivals, correcting for the regional ocean bottom slope (about 0.4 degrees).

5. Correction of the water-wave signal intensities for (a) spherical spreading along the ray-traced travel path, (b) source level, (c) receiver response, and (d) surface decoupling loss (Bannister and Pedersen, 1981).

6. Interpolation of water-wave signal intensities at integer grazing angles between the limits of the data.

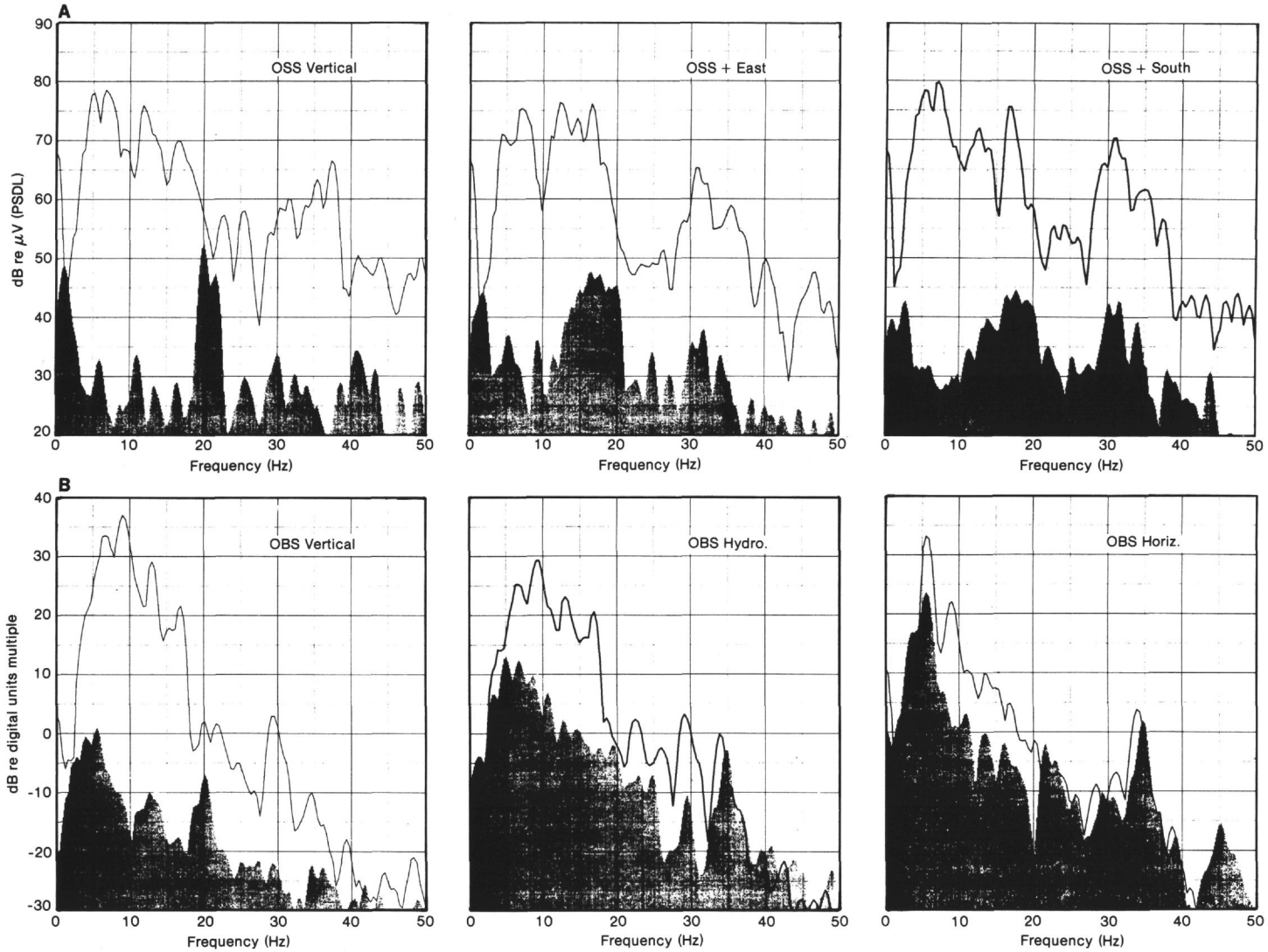

Figure 10. A. OSS IV signal and noise spectra from Shot #503. All spectra shown are for signals and noise (shaded region) prior to the onset of the water wave. All spectra are generated from 2.56 s of data (256 point FFTs), and smoothed to an equivalent 1-Hz bandwidth. All signals are as recorded and are not corrected for instrument response. B. OSU OBS signal and noise spectra from Shot #503. Recorded in the same manner as Part A.

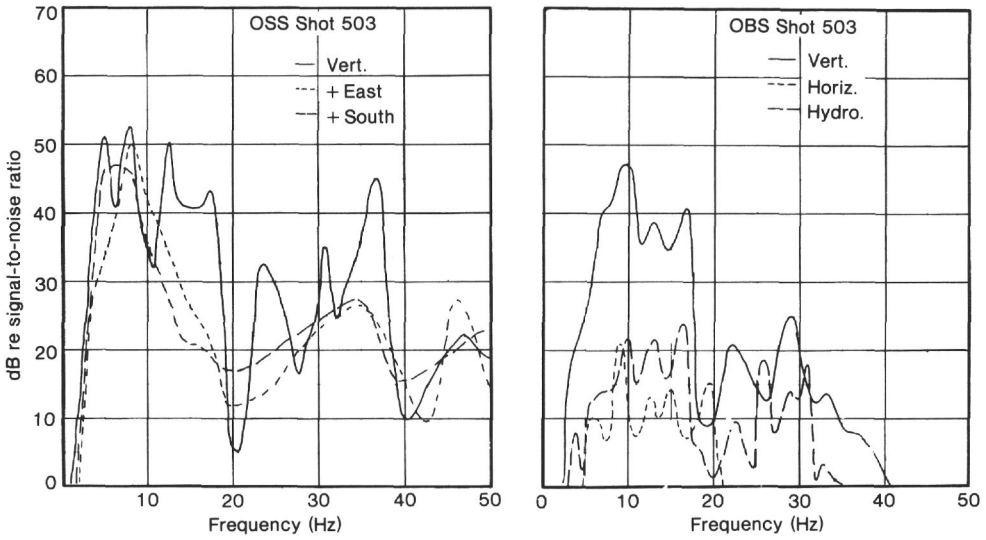

Figure 11. Signal-to-noise ratios from Shot #503 calculated for OSS IV geophones and the OSU OBS. (Bandwidth = 1 Hz.)

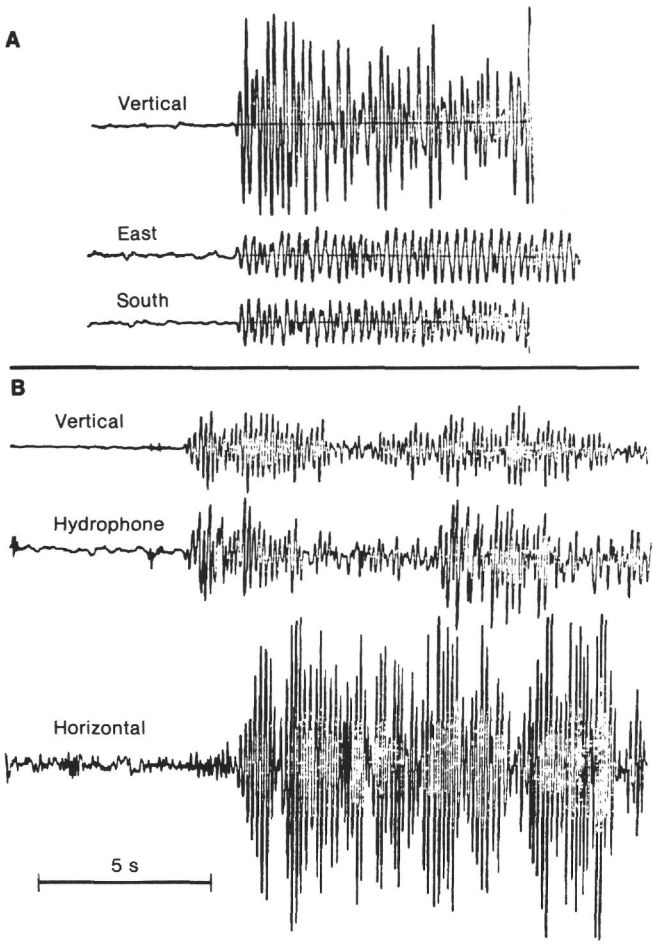

Figure 12. Signals from similar earthquakes recorded by OSS IV and an HIG OBS. A. OSS IV recording of M = 4.9 earthquake from Kamchatka at a range of 7.8° (30 Oct. 1982, 1625Z). B. OBS recording of M = 5.0 earthquake from Kuriles at a range of 8.1° (6 Sept. 1982, 0037Z). Both events are reported as normal depth (33 km). Severe clipping of the OSS horizontal geophones prevents comparison of S/N for these components.

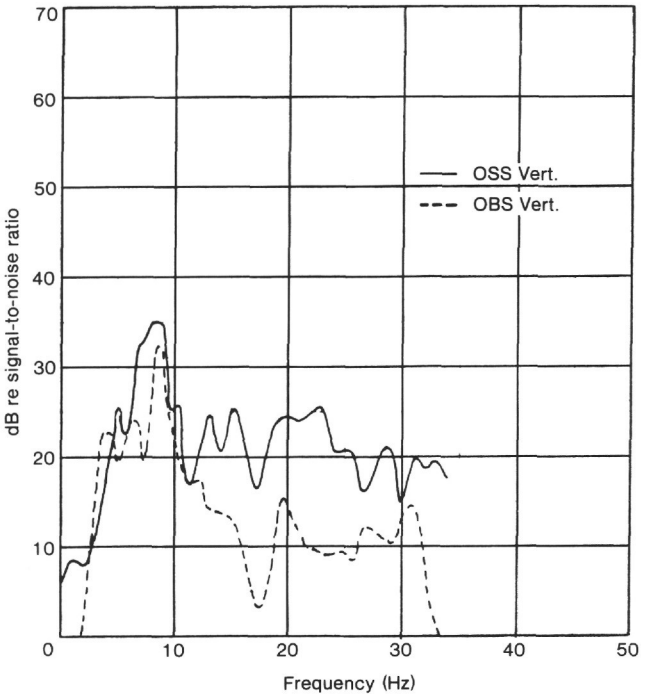

Figure 13. Signal-to-noise ratios for the vertical geophone first arrivals for the earthquakes shown in Figure 11. (Bandwidth = 1 Hz.)

These reduced data were then used to compute bottom-reflection loss and bottom transmission loss (for a detailed discussion see Fisher, 1986).

Bottom reflection loss (BRL) was computed for a frequency band (Δf) and ocean bottom grazing angle (g) as follows:

$$\mathrm{BRL}(\Delta f, g, N) = 10 \log_{10}(\mathrm{NWW}(\Delta f, g)/\mathrm{MWW}(\Delta f, g)) / (N - M(\Delta f, g)),$$

where N does not equal M. M is held constant, while N changes, to yield an independent BRL estimate for each

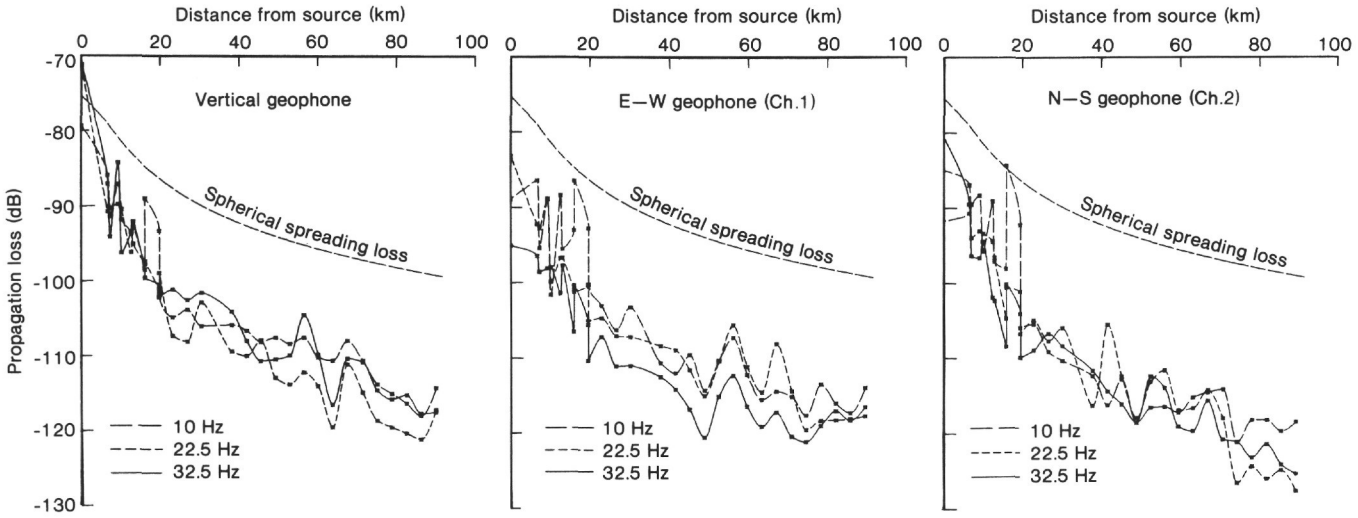

Figure 14. Propagation loss curves for OSS IV geophones obtained from SUS charge line (run approximately East-West).

N at each grazing angle and frequency band (and M has been chosen such that it is less than all N at that grazing angle and frequency band). Here NWW and MWW are the interpolated signal intensities (at grazing angle g and for a frequency band Δf) of bottom interacting rays with N and M bottom interactions, respectively. For example, the direct ($N = 1$) arrival has one bottom interaction (transmission through the bottom), the second order ($N = 2$) arrival has two bottom interactions (one reflection off the bottom and then transmission through the bottom to the receiver). The BRL values obtained for several frequency bands are shown in Figure 15. Bottom reflection loss is a well known quantity in the literature and our BRL results are similar to results found in other deep ocean sites (e.g., Santaniello et al., 1979; Mitchell et al., 1980; Chapman, 1983).

Bottom transmission loss (BTL) was computed in a way similar to BRL above using the same symbols, terms and conditions (with the addition that both N and M must be greater than one) in the following expression,

$$\mathrm{BTL}(\Delta f,g,N) = 10 \times \log_{10}((\mathrm{NWW}(\Delta f,g)^{(M(\Delta f,g)-1)})/(\mathrm{MWW}(\Delta f,g)^{(N-1)}))/(N - M(\Delta f,g))$$

Another independent estimate of bottom transmission loss is simply the corrected direct water-wave signal intensity (MWW where $M = 1$). The BTL results obtained for several frequency bands are shown in Figure 16. Ocean bottom transmission loss has not been discussed in the literature, so we cover it briefly below.

Possible causes of bottom transmission loss (BTL) include reflection from the water/sediment interface, scattering from inhomogeneities in the sub-bottom (including lateral variability of interfaces, such as cracks in the upper basement), anisotropy in the sediments or basalt, compressional to shear conversion at the sediment/basalt interface, evanescent decay in the basalt (compressional waves are evanescent at the receiver for ocean bottom grazing angles smaller than about 60° and shear waves are also evanescent there for grazing angles smaller than about 35°). The BTL term may also include other (uncorrected) effects that do not depend on the number of bottom bounces.

Comparing BTL (Fig. 16) with BRL (Fig.15) can aid in understanding both of these bottom interaction loss measures. At small grazing angles BTL is high and BRL is low. This means that at grazing angles where the ocean bottom is opaque to acoustic waves it is also a good reflector of these waves. Similarly, the combination of low BTL and high BRL at large grazing angles means that at angles where the ocean bottom is transparent to these waves it is a also poor reflector of them. Both of these conclusions make sense, since energy must be conserved throughout.

The negative BTL values in Figure 16 at high grazing angles for some frequency bands are clearly wrong, because the ocean bottom cannot amplify the signal. Since BRL and BTL are both computed from the same quantities, an error in BTL implies there is also an error in BRL at the same grazing angle and frequency. Figure 15 shows high bottom-reflection loss at these same grazing angles. A component of the high BRL values observed at high grazing angles must be erroneous. The error is probably caused by interference of sediment reverberating rays and upper basement turning rays with the specular signal arrivals. The contribution of these nonspecular rays makes the ocean bottom seem to amplify the signal, leading to lowered BTL values at high grazing angles.

This interference would also increase BRL values at the same high grazing angles. The water wave with fewer bottom bounces contains more of the interference than the water wave with a greater number of bottom bounces, due to attenuation of the reverberating and turning rays (the attenuation is caused by multiple sub-bottom reflections and intrinsic attenuation in the sub-bottom, respectively). The extra contribution of these rays to the water wave with fewer bottom bounces results in an apparent increase in bottom reflection loss via the BRL equation. BTL has a greater anomaly than BRL because the equation for BTL involves raising MWW (the intensity of the water wave with fewer bounces) to a higher

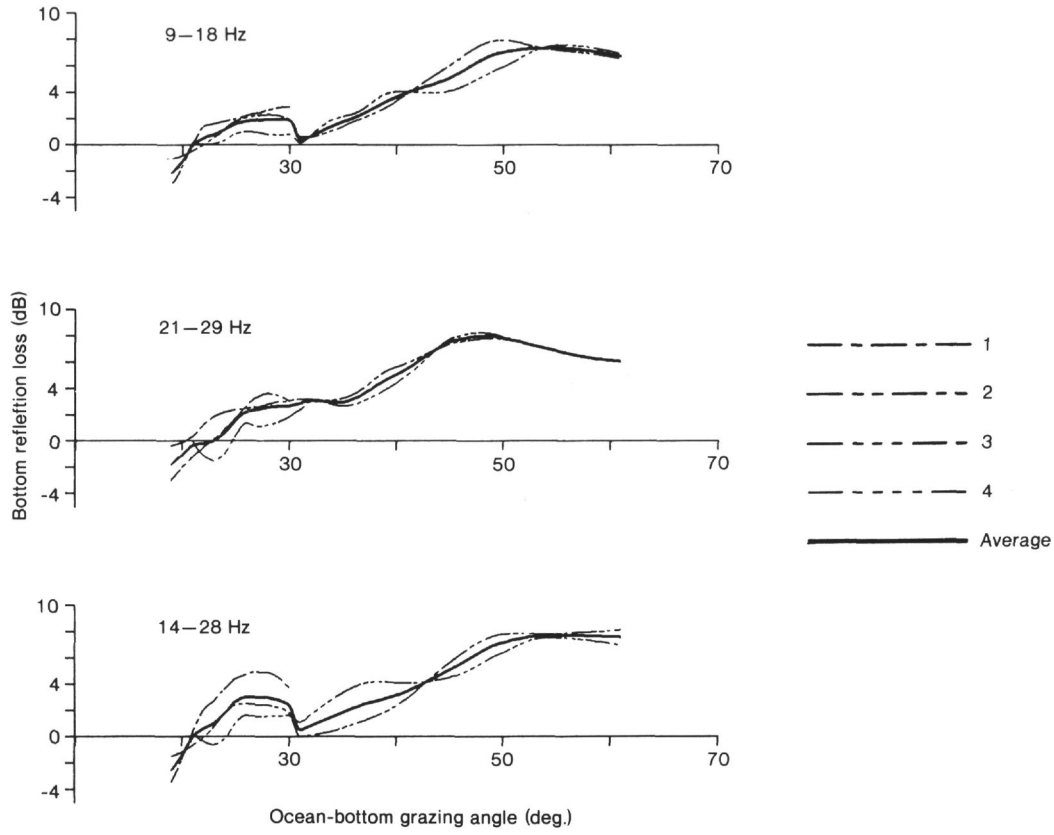

Figure 15. Bottom reflection loss (BRL) for the frequency bands 9–18, 21–29, and 14–28 Hz. Individual curves were obtained from water waves with different numbers of bottom bounces, as indicated in the key. The heavy curve is a weighted average, using signal-to-noise ratios as weights.

power than NWW is raised to. This increases the contribution of the nonspecular rays in MWW to the BTL result, leading to the anomalously low BTL at high grazing angles. (The BRL equation does not involve raising NWW and MWW to different powers.)

The cause of the unusually high propagation loss pointed out in reference to Figure 14 can now be addressed. To our knowledge, propagation loss has not previously been computed from borehole data. BTL must contribute to propagation loss measured with a borehole receiver. (BTL = 0 when the receiver is located in the water column or on the ocean floor.) Consequently, propagation loss measured in a borehole should be greater than when it is measured in the water column or on the bottom. Thus, we conclude that the observed high propagation loss is caused by transmission losses as the specular acoustic water wave travels from the water column down to the reciever in the borehole. These transmission losses are contained in the quantity BTL.

It is possible that the extra propagation loss seen in Figure 14 is partly a result of experimental error. (Errors which do not depend on the number of reflections will appear in the BTL term, as noted above.) Examples of possible sources of error include incorrect source level or receiver calibration curves (the latter possibly caused by the unexpectedly low signal levels encountered in the borehole) and incorrect source depths (which would lead to an incorrect surface decoupling loss correction).

Earlier in this chapter, we pointed out that putting the receiver in the borehole seemed to lower both the acoustic signal level and the noise level. This lowered signal level led to the observed high propagation loss values. BTL is a quantitative measure of the acoustic signal level depression (as a function of grazing angle and frequency) observed in this experiment. More propagation loss experiments with borehole receivers are needed to corroborate the BTL values found in this study and to investigate the possibility of using BTL to deduce ocean-bottom structural properties.

CONCLUSIONS

Emplacement of seismic sensors in deep ocean drill holes can enhance detectability of earthquakes and acoustic events beyond that possible using ocean bottom sensors. Water-borne acoustic signals generated in surface-limited ocean are almost certainly better detected by hydrophones in the sound channel. However, acoustic signals in shallow bottom-limited areas may be better detected by geophones buried in the ocean or in boreholes. In the surface-limited case, much of the acoustic energy is refracted upwards before it arrives at the ocean bottom, or is reflected by the ocean floor. In the bottom-limited case, much more acoustic energy can enter the ocean floor.

The removal of geophones from the ocean floor to hard rock in oceanic basement can greatly improve coup-

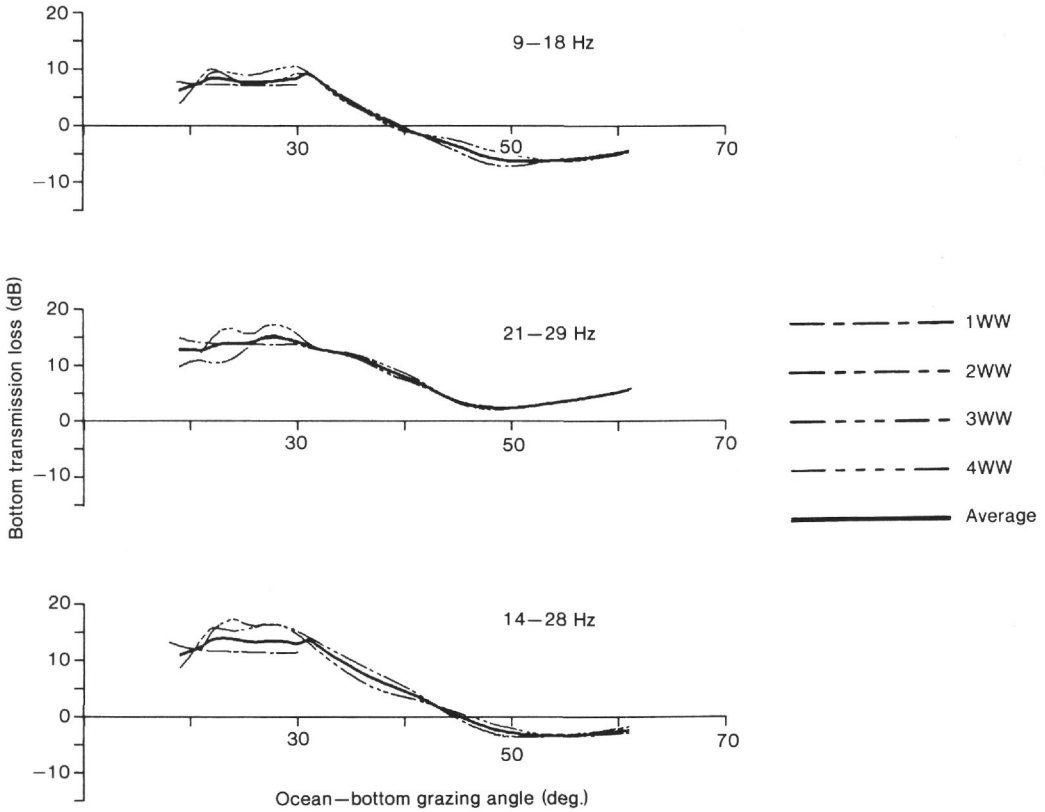

Figure 16. Bottom transmission loss (BTL) for the frequency bands 9–18, 21–29, and 14–28 Hz. Individual curves were obtained from water waves with different numbers of bottom interactions, as indicated in the key (MWW is from the BTL equation, indicating a wave with *M* bottom interactions). The heavy curve is a weighted average, using signal-to-noise ratios as weights.

ling and reduce signal complexity over that obtained from ocean-bottom seismic sensors. While vertical signal-to-noise ratios in the borehole and on the ocean floor are similar, horizontal signal-to-noise ratios are improved by more than 10 dB in the borehole because of shear-wave trapping and amplification in the sediments.

Open questions worthy of pursuing include:

1. Seismic signals: Is it profitable to emplace seismic systems in deep ocean boreholes to record earthquakes and explosions at very low frequencies (<0.1 Hz) when compared to island stations and ocean bottom seismometers?

2. What are the effects of depth of burial? Must sensors be in basement rocks to achieve optimal results? How do detectability of acoustic signals and noise level change with depth of burial?

3. What are the effects of the water column? Will buried sensors detect acoustic signals better than hydrophones in the water in bottom-limited cases?

4. How will hydrophones respond in boreholes and when buried in the sediments?

5. What are the effects of variable bottom and subbottom structures on detectability?

Results from the OSS IV experiment, combined with those of the MSS 1983 experiment, while not yet complete, will not be able to answer the above questions, and other experiments are needed.

ACKNOWLEDGMENTS

This research was funded by the Office of Naval Research through contracts with the Hawaii Institute of Geophysics and Hawaii Applied Research, Inc. We thank reviewers J. A. Carter and R. Adair for their valuable suggestions and comments. We wish to thank Rita Pujalet and Diane Henderson for their editorial assistance. Hawaii Institute of Geophysics contribution No. 1666.

REFERENCES

Adair, R. G., Orcutt, J., and Jordan, T., 1984. Analysis of ambient seismic noise recorded by downhole and ocean bottom seismometers on Deep Sea Drilling Project Leg 78B. *In* Hyndman, R. D., Salisbury, R. H., et at., *Init. Repts. DSDP*, 78B: Washington (U.S. Govt. Printing Office), 767–782.

Anderson, P. N., Duennebier, F. K., and Cessaro, R. K., in press. Horizontal seismic sensor orientation in an ocean borehole, determined from explosive charges. *J. Geophys. Res.*

Bannister, R. W., and Pedersen, M. A., 1981. Low-frequency surface interference effects in long-range sound propagation. *J. Acoust. Soc. Am.*, 69(1):76–83.

Byrne, D., Sutton, G., Blackinton, G., and Duennebier, F., 1983. Isolated sensor ocean bottom seismometer. *Mar. Geophys. Res.*, 5: 437–449.

Carter, J., Duennebier, F., and Hussong, D., 1984. A comparison between a downhole seismometer and a seismometer on the ocean floor. *Bull. Seism. Soc., Am.*, 74:763–772.

Chapman, N. R., 1983. Modeling ocean-bottom reflection loss measurements with the plane-wave reflection coefficient, *J. Acoust. Soc. Am.*, 73(5):1601–1607.

Duennebier, F. K., Cessaro, R. K., and Anderson, P. N., in press. Geoacoustic noise levels in a deep ocean borehole. *Ocean Seismo-Acoustics:* New York (Plenum Press).

Fisher, C. A., 1986. Acoustic bottom loss in the N.W. Pacific Basin; an application of a new computational method to data from a borehole receiver with a near-surface source. University of Hawaii, Manoa.

Herrin, E., 1982. The resolution of seismic instruments used in treaty verification research. *Bull. Seism. Soc. Am.*, 72B:S61–S67.

Mitchell, S. K., Bedford, N. R., and Ellis, G. E., 1980. Multipath analysis of explosive source signals in the ocean. *J. Acoust. Soc. Am.*, 67(5):1590–1597.

Nichols, R. H., 1981. Infrasonic ambient ocean noise measurements: Eleuthera. *J. Acoust. Soc. Am.*, 69:974–981.

Northrop, J., Cummings, W. C., and Morrison, M. F., 1971. Underwater 20-Hz signals recorded near Midway Island. *J. Acoust. Soc. Am.*, 49:1909–1910.

Santaniello, S. R., DiNapoli, F. R., Dullea, R. K., and Herstein, P. D., 1979. Studies on the interaction of low frequency acoustic signals with the ocean bottom. *Geophysic*, 44:1922–1940.

Urick, R. J., 1983. *Principles of Underwater Sound for Engineers* (3rd ed.): New York (McGraw Hill, Inc.).

Weston, D., 1960. Underwater explosions as acoustic sources. *Proc. Phys. Soc. London*, 76:233.

APPENDIX

Computation of Absolute Noise Levels and Propagation Loss

Calculation of absolute noise levels from OSS IV seismic data recorded on the analog cassettes is relatively straightforward. Note that for the analog-recorded data, the Nyquist frequency is 25 Hz (as opposed to 50 Hz for real-time data recorded on site when power is fed to the instrument through the cable). Automatic gain control gains are allowed to change in 12-dB steps every minute on the minute if the noise level warrants a change. The gain level is recorded as part of the time code (Ch. 1 (E–W): sec 50–52, Ch. 2 (N–S): sec 53–55, Ch. 4 (Vert): sec 56–58). Gain applied (B (g)) is shown below for each gain step:

g	B(g) (dB)
0	4
1	16
2	28
3	40
4	52
5	64
6	76
7	88

The noise-versus-time data, shown in Figure 4, were processed through an H-P 3582-A Spectrum Analyzer directly from the cassettes. As the cassettes are recorded at a rate 350 times slower than they are played back, frequencies on playback are 350 times those recorded, and 1 hr. goes by in slightly over 10 s. The Spectrum Analyzer was set at the 10-kHz scale, uniform passband, two-channel, averaging four spectra per output. At this scale each spectrum takes a time sample 12.8 ms in length (4.5 s of OSS time). One output cycle required 4.8 s, thus one spectral estimate (average of four, 4.8-s FFt's) was made every 28 min. of OSS time. As the band pass at these settings is 80 Hz (0.229 Hz, OSS frame), a 6.4-dB band-width correction was applied. These data were recorded on digital tape for later plotting.

Signal levels vary in the analog recording and playback process. The best way to determine this gain factor is as follows:

1. Measure the maximum p–p amplitude of the time code (Channel 3).
2. Multiply by 0.75 to obtain the equivalent unmodulated square-wave amplitude.
3. Divide by 4.23 V (the p–p equivalent square-wave time code amplitude at the input to the cassette).

The resulting value is the net gain (or loss) in the record–playback process.

To compute propagation loss, we know that the spectral level output by our FFT, $|X(j)|$,

$$\left[\text{defined by } X(j) = \frac{1}{N}\sum_{k=0}^{N-1} x(k)e^{-i2\pi jk/N}\right]$$

is equal to 2/2 times the rms value of the time series (in digital units) in the band represented by the $X(j)$, that is,

$$\text{rms}(\mu\text{V}) = \sqrt{2}|X(j)| \qquad \text{(for 1 digital unit = 1 } \mu\text{V).}$$

To find the average particle velocity rms $u = \bar{u}$, we must divide by the conversion factor, $C(j)$, in μV/cm/s taken from the calibration curve for the system. Note that $C(j)$, like $X(j)$, is a function of frequency where j has a one-to-one correspondence with some frequency.

$$\bar{u} = \sqrt{2}\,|X(j)|\,\frac{1}{C(j)}$$

But what we want to find is the energy-flux-density, E_0, of our observed signal {E_0 for E observed} defined by:

$$E_0 = \frac{1}{\rho_0 c_0}\int_0^\infty p_0^2(t)dt$$

$$= \frac{1}{\rho_0 c_0}\int_{t_0}^{t_1} p_0^2(t)dt$$

where the entire signal of interest lies between times t_0 and t_1.

If we know the mean-squared value of $p_0(t)$ between t_0 and t_1, $\overline{p_0^2}$, we can define E_0 by:

$$E_0 = \frac{1}{\rho_0 c_0}\,\overline{p_0^2}(t_1 - t_0)$$

Assuming that pressure can be converted to particle velocity by the following expression, $P = \rho cu$, then

$$E_0 = \rho_0 c_0 \overline{u^2}\,\Delta t \qquad (\text{for } \Delta t = t_1 - t_0)$$

Substituting for u gives:

$$E_0(j) = \rho_0 c_0\, 2|X(j)|^2\,\frac{1}{C^2(j)}\,\Delta t$$

And taking the $\log_{10}$ of both sides and multiplying by 10 yields:

$$10\log_{10}E_0(j) = 10\log_{10}|X(j)|^2 - 10\log_{10}C^2(j) + 10\log_{10}(\rho_0 c_0 2\Delta t)$$

If we define the propagation loss (actually the propagation gain): $P = E_0/E_s$ where E_s is the energy-flux-density at some place near to the source, then

$$10\log_{10}P(j) = 10\log_{10}E_0(j) - 10\log_{10}E_s(j)$$

$$= 10\log_{10}|X(j)|^2 - 10\log_{10}C^2(\text{j})$$

$$+ 10\log_{10}(\rho_0 c_0 2\Delta t) - 10\log_{10}E_s(j)$$

Taking a look at each term:

$10\log_{10}|x(j)|^2$ is the dB power level out of our spectrum program re 1 digital unit, or 1 μV,

$10\log_{10}C^2(j) = 20\log_{10}C(j)$ is the dB response of the system re μV/(cm/s), and

$10\log_{10}(\rho_0 c_0 2\Delta t\}$ = $10\log_{10}$ [(2.3 g/cm^2)(3 × 10^5 cm/s)(2)(20.48 s)]

The energy-flux-density of the source, ($10\log_{10}E_s$), must be calculated for each source used, or using the method of Weston (1960).

Values for changing OSS IV geophone output in microvolts (1 digital unit = 0.61 μV) are given in Appendix Table 1, together with conversions to other reference units.

Table 1. Transfer functions.[a]

Frequency (Hz)	Particle velocity (nm/s) (PSDL)[b]	Displacement (nm) (PSDL)[b]	Pressure at OSS in basalt (dynes/cm^2) (ρ = 2.3, c = 3.0) (PSDL)[b]	Propagation loss to OSS (MK64[c] at 1 yd.)
1	05.7	21.7	28.9	86.2
4	29.7	57.7	52.9	124.0
5	32.7	62.6	55.9	130.2
6	33.7	65.2	56.9	132.6
9	33.2	68.2	56.4	136.3
13	31.5	69.7	54.7	137.8
16	29.9	69.9	53.1	138.6
20	27.9	69.9	51.1	141.4
22	27.0	69.8	50.2	142.1
27	25.3	69.9	48.5	142.8
30	24.3	69.8	47.5	139.8
50	20.0	69.9	43.2	121.5

[a] The numbers in this table are used the convert the output of the OSS IV geophones into useful units. The numbers in each column (after the first column) are in dB such that, when subtracted from a power spectral estimate (1-Hz bandwidth) in dB re 1 V at that frequency, the resulting number is in dB referenced to the units given at the top of the column. Note that one digital unit of the OSS IV system is equal to 0.61 V.

[b] PSDL = power spectral density level, defined as the average power in a 1-Hz band in dB referenced to the units given.

[c] MK64 = Mark 64 SUS charge. 0.2-oz. explosive charge detonated at 60 ft. below the ocean surface.